

RASTER GRID PATHOLOGY AND THE CURE

ALBERT FANNJIANG

ABSTRACT. Blind ptychography is a phase retrieval method using multiple coded diffraction patterns from different, overlapping parts of the unknown extended object illuminated with an unknown window function. The window function is also known as the probe in the optics literature. As such blind ptychography is an inverse problem of simultaneous recovery of the object and the window function given the intensities of the windowed Fourier transform and has a multi-scale set-up in which the probe has an intermediate scale between the pixel scale and the macro-scale of the extended object. Uniqueness problem for blind ptychography is analyzed rigorously for the raster scan (of a constant step size τ) and its variants, in which another scale comes into play: the overlap between adjacent blocks (the shifted windows). The block phases are shown to form an arithmetic progression and the complete characterization of the raster scan ambiguities is given, including: First, the periodic raster grid pathology of degrees of freedom proportional to τ^2 and, second, a non-periodic, arithmetically progressing phase shift from block to block. Finally irregularly perturbed raster scans are shown to remove all ambiguities other than the inherent ambiguities of the scaling factor and the affine phase ambiguity under the minimum requirement of roughly 50% overlap ratio.

1. INTRODUCTION

In the last decade, ptychography has made rapid technological advances and developed into a powerful lensless coherent imaging method [18, 36, 40]. Ptychography collects the diffraction patterns from overlapping illuminations of various parts of the unknown object using a localized coherent source (the probe) [27, 30, 31], and builds on the advances in synthetic aperture methods to extend phase retrieval to unlimited objects and enhance imaging resolution [5, 19, 25, 26, 29]. Blind ptychography goes a step further and seeks to reconstruct both the unknown object and the unknown probe simultaneously [28, 35].

Mathematically, blind ptychography is an inverse problem of simultaneous recovery of the object and the window function (the probe) given the intensities of the windowed Fourier transform. In ptychography, the window function has an intermediate scale between the pixel scale and the macro-scale of the extended object.

The performance of ptychography depends on factors such as the type of illumination and the measurement scheme, including the amounts of overlap and probe positions. For example, the use of randomly structured illuminations can improve ptychographic reconstruction over that with regular illuminations [3, 7, 8, 10, 11, 16, 21, 29, 32–34, 38, 39]. Experiments suggest an overlap ratio of at least 50%, typically 60-70% between adjacent illuminations for blind ptychography [2, 22]. Optimizing the scan pattern can significantly improve the performance of ptychography and is an important part of the experimental design.

In particular, empirical evidences repeatedly point to the pitfalls of the raster scan, which is experimentally the easiest to implement [14]. Mathematically speaking, blind ptychography with raster scan seeks to recover both the object and the window function (the probe) as unknowns but only the 2D windowed Fourier *intensities* (coded diffraction patterns) as the data. Raster scanning refers to the positions of the window function. The raster scan scheme is susceptible to periodic artifacts, known as *raster grid pathology*, attributed to the regularity and symmetry of the scan positions [35].

On the other hand, to the best of our knowledge, raster grid pathology has not been precisely formulated and analyzed. The purpose of the present work is a complete analysis of raster grid pathology from the perspective of inverse problems. Uniqueness of solution is fundamental to any inverse problem. The exceptions to uniqueness are called the ambiguities. We identify the raster grid pathology reported in optics literature as *periodic* ambiguities of period equal to the step size of the raster scan. Moreover, we will characterize all the ambiguities inherent to the raster scan ptychography and propose a simple modification that can eliminate all the ambiguities except for those inherent to *any* blind ptychography.

The first thing to note is that raster grid pathology only appears in blind ptychography but not in ptychography with a known probe. In the latter case, the only ambiguity is a constant phase factor which has no real significance (and will be ignored) and the convergence behaviors of the raster scan ptychography with a known probe has been rigorously established [3].

Second, there are two ambiguities inherent to any blind ptychography: a scaling factor and an affine phase factor. To give a precise description, we introduce some notation as follows.

Let $\mathbb{Z}_n^2 = \llbracket 0, n-1 \rrbracket^2$ be the object domain containing the support of the discrete object f where $\llbracket k, l \rrbracket$ denotes the integers between, and including, $k \leq l \in \mathbb{Z}$. Let $\mathcal{M}^{00} := \mathbb{Z}_m^2, m < n$, be the initial probe area which is also the support of the probe μ^{00} describing the illumination field. Here n is the global scale and m the intermediate scale of the set-up.

Let \mathcal{T} be the set of all shifts, including $(0, 0)$, involved in the ptychographic measurement. Denote by $\mu^{\mathbf{t}}$ the \mathbf{t} -shifted probe for all $\mathbf{t} \in \mathcal{T}$ and $\mathcal{M}^{\mathbf{t}}$ the domain of $\mu^{\mathbf{t}}$. Let $f^{\mathbf{t}}$ be the object restricted to $\mathcal{M}^{\mathbf{t}}$. We write $f = \vee_{\mathbf{t}} f^{\mathbf{t}}$ and refer to each $f^{\mathbf{t}}$ as a part of f . In ptychography, the original object is broken up into a set of overlapping object parts, each of which produces a $\mu^{\mathbf{t}}$ -coded diffraction pattern (i.e. Fourier intensity). The totality of the coded diffraction patterns is called the ptychographic measurement data. Let ν^{00} (with $\mathbf{t} = (0, 0)$) and $g = \vee_{\mathbf{t}} g^{\mathbf{t}}$ be any pair of the probe and the object estimates producing the same ptychography data as μ^{00} and f , i.e. the diffraction pattern of $\nu^{\mathbf{t}} \odot g^{\mathbf{t}}$ is identical to that of $\mu^{\mathbf{t}} \odot f^{\mathbf{t}}$ where $\nu^{\mathbf{t}}$ is the \mathbf{t} -shift of ν^{00} and $g^{\mathbf{t}}$ is the restriction of g to $\mathcal{M}^{\mathbf{t}}$. For convenience, we assume the value zero for $\mu^{\mathbf{t}}, f^{\mathbf{t}}, \nu^{\mathbf{t}}, g^{\mathbf{t}}$ outside of $\mathcal{M}^{\mathbf{t}}$ and the periodic boundary condition on \mathbb{Z}_n^2 when $\mu^{\mathbf{t}}$ crosses over the boundary of \mathbb{Z}_n^2 .

Consider the probe and object estimates

$$(1) \quad \nu^{00}(\mathbf{n}) = \mu^{00}(\mathbf{n}) \exp(-ia - i\mathbf{w} \cdot \mathbf{n}), \quad \mathbf{n} \in \mathcal{M}^{00}$$

$$(2) \quad g(\mathbf{n}) = f(\mathbf{n}) \exp(ib + i\mathbf{w} \cdot \mathbf{n}), \quad \mathbf{n} \in \mathbb{Z}_n^2$$

for any $a, b \in \mathbb{R}$ and $\mathbf{w} \in \mathbb{R}^2$. For any \mathbf{t} , we have the following calculation

$$\begin{aligned}\nu^{\mathbf{t}}(\mathbf{n}) &= \nu^{00}(\mathbf{n} - \mathbf{t}) \\ &= \mu^{00}(\mathbf{n} - \mathbf{t}) \exp(-i\mathbf{w} \cdot (\mathbf{n} - \mathbf{t})) \exp(-ia) \\ &= \mu^{\mathbf{t}}(\mathbf{n}) \exp(-i\mathbf{w} \cdot (\mathbf{n} - \mathbf{t})) \exp(-ia)\end{aligned}$$

and hence for all $\mathbf{n} \in \mathcal{M}^{\mathbf{t}}, \mathbf{t} \in \mathcal{T}$

$$(3) \quad \nu^{\mathbf{t}}(\mathbf{n}) g^{\mathbf{t}}(\mathbf{n}) = \mu^{\mathbf{t}}(\mathbf{n}) f^{\mathbf{t}}(\mathbf{n}) \exp(i(b - a)) \exp(i\mathbf{w} \cdot \mathbf{t}).$$

Clearly, (3) implies that g and ν^{00} produce the same ptychographic data as f and μ^{00} since for each \mathbf{t} , $\nu^{\mathbf{t}} \odot g^{\mathbf{t}}$ is a constant phase factor times $\mu^{\mathbf{t}} \odot f^{\mathbf{t}}$.

In addition to the affine phase ambiguity (1)-(2), another ambiguity, a scaling factor ($g = cf, \nu^{00} = c^{-1}\mu^{00}, c > 0$), is also inherent to any blind ptychography as can easily be checked. We refer to the scaling factor and the affine phase ambiguity as the inherent ambiguities of blind ptychography. Note that when the probe is exactly known $\nu^{00} = \mu^{00}$, neither ambiguity can occur.

A recent theory of uniqueness for blind ptychography with random probes [9] establishes that for general sampling schemes and with high probability (in the selection of the random probe), we have the relation

$$(4) \quad \nu^{\mathbf{t}} \odot g^{\mathbf{t}} = e^{i\theta_{\mathbf{t}}} \mu^{\mathbf{t}} \odot f^{\mathbf{t}}, \quad \mathbf{t} \in \mathcal{T},$$

for some constants $\theta_{\mathbf{t}} \in \mathbb{R}$ (called block phases here) if g and $\nu^{\mathbf{t}}$ produce the same diffraction pattern as f and $\mu^{\mathbf{t}}$ for all $\mathbf{t} \in \mathcal{T}$. Here \odot denotes the component-wise (Hadamard) product. The masked object parts $\psi^{\mathbf{t}} := \mu^{\mathbf{t}} \odot f^{\mathbf{t}}$ are also known as the *exit waves* in the scanning transmission electron microscopy literature.

We refer to (4) as the *local uniqueness* of the exit waves which means unique determination of the exit waves up to the block phases but not globally since $\theta_{\mathbf{t}}$ can depend on \mathbf{t} and vary from block to block. However, the block phase profile is not arbitrary. For example, block phases for the raster scan and the perturbed raster scan always form an arithmetic progression (see below), possessing two degrees of freedom.

Once the exit waves $\psi^{\mathbf{t}}$ are determined up to block phases, (4) with $\theta_{\mathbf{t}}$ treated as parameters represents a bilinear system (in ν^{00} and g) of $m^2 \times |\mathcal{T}|$ equations coupled through the overlap between adjacent blocks. The total number of complex variables is $n^2 + m^2$. In the case of raster scan with step size τ , $|\mathcal{T}| \approx n^2/\tau^2$ and $m^2|\mathcal{T}| \approx n^2(\tau/m)^{-2}$ where the shift ratio τ/m is 1 minus the overlap ratio $(m - \tau)/m$. For 50% overlap ratio and $m < n$, $m^2|\mathcal{T}| \approx 4n^2$, a couple times larger than $(n^2 + m^2)$. This speaks of the potential redundancy of information in (4) on dimension count. Yet this simplistic analysis is deceptive as we will see that due to degenerate coupling the raster scan has ambiguities of exactly $\tau^2 + 2$ degrees of freedom in addition to the three degrees of freedom of the inherent ambiguities discussed above.

We will take (4) as the starting point of our analysis of raster scan ambiguities, first to characterize all the ambiguities in the raster scan and, second, to show how to harness the nonlinear coupling in (4) by more nuanced design of measurement schemes in which pixel-scale changes result in total eradication of ambiguities other than the inherent ones through the intermediate-scale coupling.

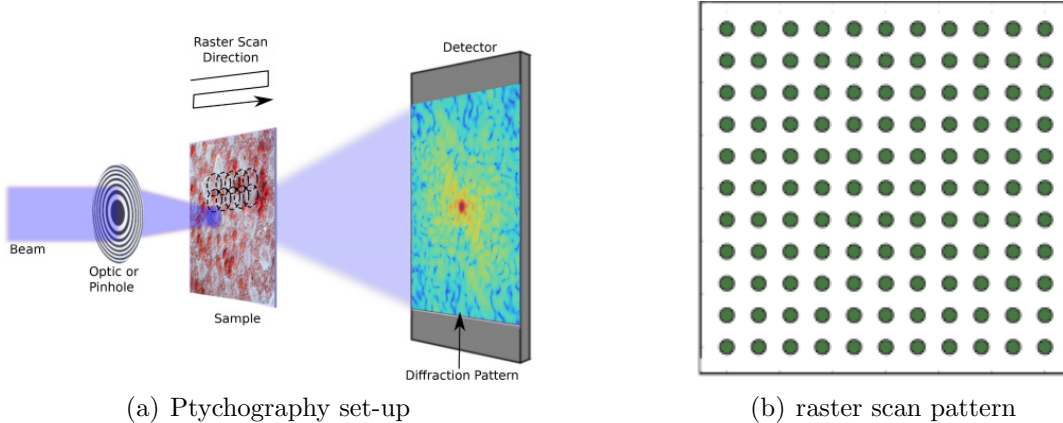


FIGURE 1. Simplified ptychographic setup showing a Cartesian grid used for the overlapping raster scan positions [24].

1.1. Our contribution. We first prove that the block phases of the raster scan of any step size $\tau < m$ always have an affine profile (Section 3, Theorem 3.1). We then give a complete characterization of the raster scan ambiguities (Theorem 4.3).

Roughly speaking, there are two types of ambiguities besides the inherent ambiguities (the scaling factor and the affine phase ambiguity (1)-(2)). First, there is the non-periodic, arithmetically progressing ambiguity, inherited from the aforementioned affine block phase profile, which varies on the block scale while the affine phase ambiguity varies on the pixel scale.

Second, there are τ -periodic ambiguities of τ^2 degrees of freedom, which we identify as mathematical description of the raster grid pathology reported in the optics literature. The larger the step size the (much) greater the degrees of ambiguity which can not be removed without extra prior information.

Finally we demonstrate a simple mechanism for eliminating all the other ambiguities than the scaling factor and the affine phase ambiguity by slightly perturbing the raster scan with the minimum overlap ratio roughly 50%, consistent with experimental findings in the optics literature (Section 5, Theorem 5.5). The optimal tradeoff between the speed of data acquisition and the convergence rate of reconstruction lies in the balance between the average step size and the overlap size.

The rest of the paper is organized as follows. In Section 2, we give a detailed presentation of the raster scan. In Section 3, we prove that the block phases have an affine profile. In Section 4, we give a complete characterization of the raster scan ambiguities. In Section 5 we show that slightly perturbed raster scan has no other ambiguities than the scaling factor and the affine phase ambiguity. In Section 6, we give numerical demonstrate of the perturbed raster scan. We conclude with a few remarks in Section 7.

2. RASTER SCAN

The raster scan can be formulated as the 2D lattice with the basis $\{\mathbf{v}_1, \mathbf{v}_2\}$

$$(5) \quad \mathcal{T} = \{\mathbf{t}_{kl} \equiv k\mathbf{v}_1 + l\mathbf{v}_2 : k, l \in \mathbb{Z}\}, \quad \mathbf{v}_1, \mathbf{v}_2 \in \mathbb{Z}^2$$

acting on the object domain \mathbb{Z}_n^2 . Instead of \mathbf{v}_1 and \mathbf{v}_2 we can also take $\mathbf{u}_1 = \ell_{11}\mathbf{v}_1 + \ell_{12}\mathbf{v}_2$ and $\mathbf{u}_2 = \ell_{21}\mathbf{v}_1 + \ell_{22}\mathbf{v}_2$ for integers ℓ_{ij} with $\ell_{11}\ell_{22} - \ell_{12}\ell_{21} = \pm 1$. This ensures that \mathbf{v}_1 and \mathbf{v}_2 themselves are integer linear combinations of $\mathbf{u}_1, \mathbf{u}_2$. Every lattice basis defines a fundamental parallelogram, which determines the lattice. There are five 2D lattice types, called period lattices, as given by the crystallographic restriction theorem. In contrast, there are 14 lattice types in 3D, called Bravais lattices [4].

We will focus on the simplest raster scan corresponding to the *square lattice* with $\mathbf{v}_1 = (\tau, 0), \mathbf{v}_2 = (0, \tau)$ of step size $\tau \in \mathbb{N}$. Our results can easily be extended to other lattice schemes.

Under the periodic boundary condition the raster scan with the step size $\tau = n/q, q \in \mathbb{N}$, \mathcal{T} consists of $\mathbf{t}_{kl} = \tau(k, l)$, with $k, l \in \{0, 1, \dots, q-1\}$. The periodic boundary condition means that for $k = q-1$ or $l = q-1$ the shifted probe is wrapped around into the other end of the object domain. Denote the \mathbf{t}_{kl} -shifted probes and blocks by μ^{kl} and \mathcal{M}^{kl} , respectively. Likewise, denote by f^{kl} the object restricted to the shifted domain \mathcal{M}^{kl} .

Depending on whether $\tau \leq m/2$ (the under-shifting case) or $\tau > m/2$ (the over-shifting case), we have two types of schemes. For the former case, all pixels of the the object participate in an equal number of diffraction patterns. For the latter case, however, $4(m-\tau)^2$ pixels participate in four, $4(2\tau-m)(m-\tau)$ pixels participate in two and $(2\tau-m)^2$ pixels participate in only one diffraction pattern, resulting in uneven coverage of the object.

2.1. The under-shifting scheme $\tau \leq m/2$. For simplicity of presentation we consider the case of $\tau = m/p$ for some integer $p \geq 2$ (i.e. $pn = qm$). As noted above, all pixels of the the object participate in the same number (i.e. $2p$) of diffraction patterns. The borderline case $\tau = m/2$ (dubbed the minimalist scheme in [3]) corresponds to $p = 2$.

We partition the cyclical \mathbf{t}^{kl} -shifted probe μ^{kl} and the corresponding domain into equal-sized square blocks as

$$(6) \quad \mu^{kl} = \begin{bmatrix} \mu_{00}^{kl} & \mu_{10}^{kl} & \cdots & \mu_{p-1,0}^{kl} \\ \mu_{01}^{kl} & \mu_{11}^{kl} & \cdots & \mu_{p-1,1}^{kl} \\ \vdots & \vdots & \vdots & \vdots \\ \mu_{0,p-1}^{kl} & \mu_{1,p-1}^{kl} & \cdots & \mu_{p-1,p-1}^{kl} \end{bmatrix}, \quad \mu_{ij}^{kl} \in \mathbb{C}^{m/p \times m/p}$$

$$(7) \quad \mathcal{M}^{kl} = \begin{bmatrix} \mathcal{M}_{00}^{kl} & \mathcal{M}_{10}^{kl} & \cdots & \mathcal{M}_{p-1,0}^{kl} \\ \mathcal{M}_{01}^{kl} & \mathcal{M}_{11}^{kl} & \cdots & \mathcal{M}_{p-1,1}^{kl} \\ \vdots & \vdots & \vdots & \vdots \\ \mathcal{M}_{0,p-1}^{kl} & \mathcal{M}_{1,p-1}^{kl} & \cdots & \mathcal{M}_{p-1,p-1}^{kl} \end{bmatrix}, \quad \mathcal{M}_{ij}^{kl} \in \mathbb{Z}^{m/p \times m/p}$$

under the periodic boundary condition

$$(8) \quad \mu_{j,l}^{q-1-i,k} = \mu_{j-i-1,l}^{0k}, \quad \mu_{l,j}^{k,q-1-i} = \mu_{l,j-i-1}^{k0},$$

$$(9) \quad \mathcal{M}_{j,l}^{q-1-i,k} = \mathcal{M}_{j-i-1,l}^{0k}, \quad \mathcal{M}_{l,j}^{k,q-1-i} = \mathcal{M}_{l,j-i-1}^{k0}$$

for all $0 \leq i \leq j-1 \leq p-2, k=1, \dots, q-1, l=1, \dots, p-1$.

Accordingly, we divide the object f into q^2 non-overlapping square blocks

$$(10) \quad f = \begin{bmatrix} f_{00} & \cdots & f_{q-1,0} \\ \vdots & \vdots & \vdots \\ f_{0,q-1} & \cdots & f_{q-1,q-1} \end{bmatrix}, \quad f_{ij} \in \mathbb{C}^{m/p \times m/p}.$$

2.2. The over-shifting scheme $\tau > m/2$. Because of uneven coverage of the object domain, the over-shifting case is more complicated.

We divide the shifted probe μ^{kl} and its domain as

$$(11) \quad \mu^{kl} = \begin{bmatrix} \mu_{00}^{kl} & \mu_{10}^{kl} & \mu_{20}^{kl} \\ \mu_{01}^{kl} & \mu_{11}^{kl} & \mu_{21}^{kl} \\ \mu_{02}^{kl} & \mu_{12}^{kl} & \mu_{22}^{kl} \end{bmatrix} \in \mathbb{C}^{m \times m}$$

$$(12) \quad \mathcal{M}^{kl} = \begin{bmatrix} \mathcal{M}_{00}^{kl} & \mathcal{M}_{10}^{kl} & \mathcal{M}_{20}^{kl} \\ \mathcal{M}_{01}^{kl} & \mathcal{M}_{11}^{kl} & \mathcal{M}_{21}^{kl} \\ \mathcal{M}_{02}^{kl} & \mathcal{M}_{12}^{kl} & \mathcal{M}_{22}^{kl} \end{bmatrix} \in \mathbb{Z}^{m \times m}$$

under the periodic boundary condition

$$(13) \quad \mathcal{M}_{2j}^{q-1,k} = \mathcal{M}_{0j}^{0k}, \quad \mathcal{M}_{i2}^{k,q-1} = \mathcal{M}_{i0}^{k0}$$

$$(14) \quad \mu_{2j}^{q-1,k} = \mu_{0j}^{0k}, \quad \mu_{i2}^{k,q-1} = \mu_{i0}^{k0},$$

for all $k=1, \dots, q-1$ and $i, j=0, 1, 2$, where q is the number of shifts in each direction.

Note that the sizes of these blocks are not equal: the four corner blocks are $(m-\tau) \times (m-\tau)$, the center block is $(2\tau-m) \times (2\tau-m)$ and the rest are either $(2\tau-m) \times (m-\tau)$ or $(m-\tau) \times (2\tau-m)$. As a result, the corresponding partition of f also has unequally sized blocks.

We write

$$(15) \quad f = \bigvee_{k,l=0}^{q-1} f^{kl}, \quad f^{kl} = \begin{bmatrix} f_{00}^{kl} & f_{10}^{kl} & f_{20}^{kl} \\ f_{01}^{kl} & f_{11}^{kl} & f_{21}^{kl} \\ f_{02}^{kl} & f_{12}^{kl} & f_{22}^{kl} \end{bmatrix} \in \mathbb{C}^{m \times m}$$

where, for $i, j=0, 1, 2, \quad k, l=0, \dots, q-1$,

$$f_{2j}^{kl} = f_{0j}^{k+1,l}, \quad f_{i2}^{k,l} = f_{i0}^{k,l+1}.$$

3. AFFINE BLOCK PHASES

Let S be any cyclic subgroup of \mathcal{T} generated by \mathbf{v} , i.e. $S := \{\mathbf{t}_j = j\mathbf{v} : j=0, \dots, s-1\}$, of order s , i.e. $s\mathbf{v} = 0 \pmod{n}$. For ease of notation, denote by μ^k, f^k, ν^k, g^k and M^k for the respective \mathbf{t}_k -shifted quantities.

Theorem 3.1. *As in (4), suppose that*

$$(16) \quad \nu^k(\mathbf{n})g^k(\mathbf{n}) = e^{i\theta_k}\mu^k(\mathbf{n})f^k(\mathbf{n})$$

for all $\mathbf{n} \in \mathcal{M}^k$ and $k = 0, \dots, s-1$. If, for all $k = 0, \dots, s-1$,

$$(17) \quad \mathcal{M}^k \cap \mathcal{M}^{k+1} \cap \text{supp}(f) \cap (\text{supp}(f) + \mathbf{v}) \neq \emptyset,$$

then the sequence $\{\theta_0, \theta_1, \dots, \theta_{s-1}\}$ is an arithmetic progression where $\Delta\theta = \theta_k - \theta_{k-1}$ is an integer multiple of $2\pi/s$.

Remark 3.2. *If f has a full support, i.e. $\text{supp}(f) = \mathbb{Z}_n^2$, then (17) holds for any step size $\tau < m$ (i.e. positive overlap).*

Proof. Rewriting (16) in the form

$$(18) \quad \nu^{k+1}(\mathbf{n})g^{k+1}(\mathbf{n}) = e^{i\theta_{k+1}}\mu^{k+1}(\mathbf{n})f^{k+1}(\mathbf{n})$$

and substituting (16) into (18) for $\mathbf{n} \in \mathcal{M}^k \cap \mathcal{M}^{k+1}$, we have

$$e^{i\theta_k}f^k(\mathbf{n})\mu^k(\mathbf{n})/\nu^k(\mathbf{n}) = e^{i\theta_{k+1}}\mu^{k+1}(\mathbf{n})/\nu^{k+1}(\mathbf{n})f^{k+1}(\mathbf{n})$$

and hence for all $\mathbf{n} \in \mathcal{M}^k \cap \mathcal{M}^{k+1} \cap \text{supp}(f)$,

$$(19) \quad e^{i\theta_k}\mu^k(\mathbf{n})/\nu^k(\mathbf{n}) = e^{i\theta_{k+1}}\mu^{k+1}(\mathbf{n})/\nu^{k+1}(\mathbf{n}).$$

For all $j = 0, \dots, s-1$, substituting

$$(20) \quad \nu^j(\mathbf{n}) = \nu^{j+1}(\mathbf{n} + \mathbf{v}), \quad \mu^j(\mathbf{n}) = \mu^{j+1}(\mathbf{n} + \mathbf{v}),$$

into (19), we have that for $\mathbf{n} \in \mathcal{M}^k \cap \mathcal{M}^{k+1} \cap \text{supp}(f)$

$$\begin{aligned} & e^{i\theta_k}\mu^{k+1}(\mathbf{n} + \mathbf{v})/\nu^{k+1}(\mathbf{n} + \mathbf{v}) \\ &= e^{i\theta_{k+1}}\mu^{k+2}(\mathbf{n} + \mathbf{v})/\nu^{k+2}(\mathbf{n} + \mathbf{v}), \end{aligned}$$

or equivalently

$$(21) \quad \begin{aligned} e^{i\theta_k}\mu^{k+1}(\mathbf{n})/\nu^{k+1}(\mathbf{n}) &= e^{i\theta_{k+1}}\mu^{k+2}(\mathbf{n})/\nu^{k+2}(\mathbf{n}), \\ \forall \mathbf{n} &\in \mathcal{M}^{k+1} \cap \mathcal{M}^{k+2} \cap (\text{supp}(f) + \mathbf{v}) \end{aligned}$$

On the other hand, (19) also implies

$$(22) \quad \begin{aligned} e^{i\theta_{k+1}}\mu^{k+1}(\mathbf{n})/\nu^{k+1}(\mathbf{n}) &= e^{i\theta_{k+2}}\mu^{k+2}(\mathbf{n})/\nu^{k+2}(\mathbf{n}), \\ \forall \mathbf{n} &\in \mathcal{M}^{k+1} \cap \mathcal{M}^{k+2} \cap \text{supp}(f). \end{aligned}$$

Hence, if

$$\mathcal{M}^k \cap \mathcal{M}^{k+1} \cap \text{supp}(f) \cap (\text{supp}(f) + \mathbf{v}) \neq \emptyset$$

then (22) and (21) imply that

$$(23) \quad e^{i\theta_{k+1}}e^{-i\theta_k} = e^{i\theta_k}e^{-i\theta_{k-1}}, \quad \forall k = 0, \dots, s-1$$

and hence $\Delta\theta = \theta_k - \theta_{k-1}$ is independent of k . In other words, $\{\theta_0, \theta_1, \theta_2, \dots\}$ is an arithmetic progression.

Moreover, the periodic boundary condition and the fact that $s\mathbf{v} = 0 \pmod{2\pi}$ imply that $s\Delta\theta$ is an integer multiple of 2π . \square

Applying Theorem 3.1 to the two-generator group \mathcal{T} of the raster scan we have the following result.

Corollary 3.3. *For the full raster scan \mathcal{T} , the block phases have the profile*

$$(24) \quad \theta_{kl} = \theta_{00} + \mathbf{r} \cdot (k, l), \quad k, l = 0, \dots, q-1,$$

for some $\theta_{00} \in \mathbb{R}$ and $\mathbf{r} = (r_1, r_2)$ where r_1 and r_2 are integer multiples of $2\pi/q$.

4. RASTER SCAN AMBIGUITIES

In this section we give a complete characterization of the raster scan ambiguities other than the scaling factor and the affine phase ambiguity (1)-(2), including the arithmetically progressing phase factor inherited from the block phases and the raster grid pathology which has a τ -periodic structure of $\tau \times \tau$ degrees of freedom. We will use the notation in Section 2.

Before we state the general result. Let us consider two simple examples to illustrate each type of ambiguity separately.

The first example shows an ambiguity resulting from the arithmetically progressing block phases which make positive and negative imprints on the object and phase estimates, respectively.

Example 4.1. *For $q = 3, \tau = m/2$, let*

$$\begin{aligned} f &= \begin{bmatrix} f_{00} & f_{10} & f_{20} \\ f_{01} & f_{11} & f_{21} \\ f_{02} & f_{12} & f_{22} \end{bmatrix} \\ g &= \begin{bmatrix} f_{00} & e^{i2\pi/3} f_{10} & e^{i4\pi/3} f_{20} \\ e^{i2\pi/3} f_{01} & e^{i4\pi/3} f_{11} & f_{21} \\ e^{i4\pi/3} f_{02} & f_{12} & e^{i2\pi/3} f_{22} \end{bmatrix} \end{aligned}$$

be the object and its reconstruction, respectively, where $f_{ij} \in \mathbb{C}^{n/3 \times n/3}$. Let

$$\mu^{kl} = \begin{bmatrix} \mu_{00}^{kl} & \mu_{10}^{kl} \\ \mu_{01}^{kl} & \mu_{11}^{kl} \end{bmatrix}, \quad \nu^{kl} = \begin{bmatrix} \mu_{00}^{kl} & e^{-i2\pi/3} \mu_{10}^{kl} \\ e^{-i2\pi/3} \mu_{01}^{kl} & e^{-i4\pi/3} \mu_{11}^{kl} \end{bmatrix},$$

$k, l = 0, 1, 2$, be the (k, l) -th shift of the probe and estimate, respectively, where $\mu_{ij}^{kl} \in \mathbb{C}^{n/3 \times n/3}$.

Let f^{ij} and g^{ij} be the part of the object and estimate illuminated by μ^{ij} and ν^{ij} , respectively. It is verified easily that $\nu^{ij} \odot g^{ij} = e^{i(i+j)2\pi/3} \mu^{ij} \odot f^{ij}$.

The next example illustrates the periodic artifact called raster grid pathology.

Example 4.2. For $q = 3, \tau = m/2$ and any $\psi \in \mathbb{C}^{\frac{n}{3} \times \frac{n}{3}}$, let

$$\begin{aligned} f &= \begin{bmatrix} f_{00} & f_{10} & f_{20} \\ f_{01} & f_{11} & f_{21} \\ f_{02} & f_{12} & f_{22} \end{bmatrix} \\ g &= \begin{bmatrix} e^{-i\psi} \odot f_{00} & e^{-i\psi} \odot f_{10} & e^{-i\psi} \odot f_{20} \\ e^{-i\psi} \odot f_{01} & e^{-i\psi} \odot f_{11} & e^{-i\psi} \odot f_{21} \\ e^{-i\psi} \odot f_{02} & e^{-i\psi} \odot f_{12} & e^{-i\psi} \odot f_{22} \end{bmatrix} \end{aligned}$$

be the object and its reconstruction, respectively, where $f_{ij} \in \mathbb{C}^{n/3 \times n/3}$. Let

$$\mu^{kl} = \begin{bmatrix} \mu_{00}^{kl} & \mu_{10}^{kl} \\ \mu_{01}^{kl} & \mu_{11}^{kl} \end{bmatrix}, \quad \nu^{kl} = \begin{bmatrix} e^{i\psi} \odot \mu_{00}^{kl} & e^{i\psi} \odot \mu_{10}^{kl} \\ e^{i\psi} \odot \mu_{01}^{kl} & e^{i\psi} \odot \mu_{11}^{kl} \end{bmatrix},$$

$k, l = 0, 1, 2$, be the (k, l) -th shift of the probe and estimate, respectively, where $\mu_{ij}^{kl} \in \mathbb{C}^{n/3 \times n/3}$.

Let f^{ij} and g^{ij} be the part of the object and estimate illuminated by μ^{ij} and ν^{ij} , respectively. It is verified easily that $\nu^{ij} \odot g^{ij} = \mu^{ij} \odot f^{ij}$.

The combination of the above two types of ambiguity gives rise to the general ambiguities for blind ptychography with the raster scan as stated next.

Theorem 4.3. Suppose that $\text{supp}(f) = \mathbb{Z}_n^2$. Consider the raster scan \mathcal{T} and suppose that an object estimate g and a probe estimate ν^{00} satisfy the relation

$$(25) \quad \nu^{kl} \odot g^{kl} = e^{i\theta_{kl}} \mu^{kl} \odot f^{kl}, \quad \theta_{kl} = \theta_{00} + \mathbf{r} \cdot (k, l)$$

as given by Theorem 3.1.

Then the following statements hold.

(I). For $\tau \leq m/2$, if

$$(26) \quad \nu_{00}^{00} = e^{i\psi} \odot \mu_{00}^{00}, \quad \psi \in \mathbb{C}^{\tau \times \tau},$$

then

$$(27) \quad \nu_{kl}^{00} = e^{-i\mathbf{r} \cdot (k, l)} e^{i\psi} \odot \mu_{kl}^{00}, \quad k, l = 0, \dots, p-1$$

$$(28) \quad g_{kl} = e^{i\theta_{00}} e^{i\mathbf{r} \cdot (k, l)} e^{-i\psi} \odot f_{kl}, \quad k, l = 0, \dots, q-1.$$

(II). For $\tau > m/2$, if

$$(29) \quad \begin{bmatrix} \nu_{00}^{00} & \nu_{10}^{00} \\ \nu_{01}^{00} & \nu_{11}^{00} \end{bmatrix} = e^{i\psi} \odot \begin{bmatrix} \mu_{00}^{00} & \mu_{10}^{00} \\ \mu_{01}^{00} & \mu_{11}^{00} \end{bmatrix}$$

for some

$$\psi = \begin{bmatrix} \psi_{00} & \psi_{10} \\ \psi_{01} & \psi_{11} \end{bmatrix} \in \mathbb{C}^{\tau \times \tau},$$

then

$$(30) \quad \begin{bmatrix} g_{00}^{kl} & g_{10}^{kl} \\ g_{01}^{kl} & g_{11}^{kl} \end{bmatrix} = e^{i\theta_{00}} e^{i\mathbf{r} \cdot (k, l)} e^{-i\psi} \odot \begin{bmatrix} f_{00}^{kl} & f_{10}^{kl} \\ f_{01}^{kl} & f_{11}^{kl} \end{bmatrix}$$

for all $k, l = 0, \dots, q-1$. Moreover,

$$(31) \quad \nu_{2j}^{00} = e^{-ir_1} e^{i\psi_{0j}} \odot \mu_{2j}^{00}, \quad j = 0, 1$$

$$(32) \quad \nu_{j2}^{00} = e^{-ir_2} e^{i\psi_{j0}} \odot \mu_{j2}^{00}, \quad j = 0, 1$$

$$(33) \quad \nu_{22}^{00} = e^{-i(r_1+r_2)} e^{i\psi_{00}} \odot \mu_{22}^{00}$$

and hence

$$(34) \quad g_{2j}^{kl} = e^{i\theta_{00}} e^{i\mathbf{r} \cdot (k+1, l)} e^{-i\psi_{0j}} \odot f_{2j}^{kl}, \quad j = 0, 1$$

$$(35) \quad g_{j2}^{kl} = e^{i\theta_{00}} e^{i\mathbf{r} \cdot (k, l+1)} e^{-i\psi_{j0}} \odot f_{j2}^{kl}, \quad j = 0, 1$$

$$(36) \quad g_{22}^{kl} = e^{i\theta_{00}} e^{i\mathbf{r} \cdot (k+1, l+1)} e^{-i\psi_{00}} \odot f_{22}^{kl}.$$

Remark 4.4. Since ψ is any complex $\tau \times \tau$ matrix, (26) and (29) represent the maximum degrees of ambiguity over the respective initial sub-blocks. This ambiguity is transmitted to other sub-blocks, forming periodic artifacts called the raster grid pathology.

On top of the periodic artifacts, there is the non-periodic ambiguity inherited from the affine block phase profile. The non-periodic arithmetically progressing ambiguity is different from the affine phase ambiguity (1)-(2) as they manifest on different scales: the former on the block scale while the latter on the pixel scale.

Proof. (I). For $\tau \leq m/2$, recall the decomposition

$$\nu^{kl} = \begin{bmatrix} \nu_{00}^{kl} & \nu_{10}^{kl} & \cdots & \nu_{p-1,0}^{kl} \\ \nu_{01}^{kl} & \nu_{11}^{kl} & \cdots & \nu_{p-1,1}^{kl} \\ \vdots & \vdots & \vdots & \vdots \\ \nu_{0,p-1}^{kl} & \nu_{1,p-1}^{kl} & \cdots & \nu_{p-1,p-1}^{kl} \end{bmatrix}, \quad g = \begin{bmatrix} g_{00} & \cdots & g_{q-1,0} \\ \vdots & \vdots & \vdots \\ g_{0,q-1} & \cdots & g_{q-1,q-1} \end{bmatrix},$$

with $\nu_{ij}^{kl}, g_{ij} \in \mathbb{C}^{m/p \times m/p}$, in analogy to (6) and (10).

$$g_{00} = e^{i\theta_{00}} e^{-i\psi} \odot f_{00}$$

by restricting (25) to \mathcal{M}_{00}^{00} .

For $\mathbf{n} \in \mathcal{M}_{00}^{10}$, we have

$$\nu_{00}^{10} \odot g_{10} = e^{i\theta_{10}} \mu_{00}^{10} \odot f_{10},$$

by (25), and

$$\nu_{00}^{10}(\mathbf{n}) = \nu_{00}^{00}(\mathbf{n} - (\tau, 0)) = (e^{i\psi} \odot \mu_{00}^{00})(\mathbf{n} - (\tau, 0)) = (e^{i\psi} \odot \mu_{00}^{10})(\mathbf{n})$$

by (26). Hence

$$g_{10} = e^{i\theta_{10}} e^{-i\psi} \odot f_{10}$$

implying

$$\nu_{10}^{00} \odot g_{10} = e^{i\theta_{10}} e^{-i\psi} \nu_{10}^{00} \odot f_{10} = e^{i\theta_{00}} \mu_{10}^{00} \odot f_{10}$$

by (25) and consequently

$$\nu_{10}^{00} = e^{i\theta_{00}} e^{-i\theta_{10}} e^{i\psi} \mu_{10}^{00}.$$

Repeating the same argument for the adjacent blocks in both directions, we obtain

$$\begin{aligned}\nu_{kl}^{00} &= e^{i\theta_{00}} e^{-i\theta_{kl}} e^{i\psi} \odot \mu_{kl}^{00} \\ g_{kl} &= e^{i\theta_{kl}} e^{-i\psi} \odot f_{kl}\end{aligned}$$

which are equivalent to (27) and (28) in view of the block phase profile in (24).

(II). First recall

$$\mu^{kl} = \begin{bmatrix} \mu_{00}^{kl} & \mu_{10}^{kl} & \mu_{20}^{kl} \\ \mu_{01}^{kl} & \mu_{11}^{kl} & \mu_{21}^{kl} \\ \mu_{02}^{kl} & \mu_{12}^{kl} & \mu_{22}^{kl} \end{bmatrix}, \quad g = \bigvee_{k,l=0}^{q-1} g^{kl}, \quad g^{kl} = \begin{bmatrix} g_{00}^{kl} & g_{10}^{kl} & g_{20}^{kl} \\ g_{01}^{kl} & g_{11}^{kl} & g_{21}^{kl} \\ g_{02}^{kl} & g_{12}^{kl} & g_{22}^{kl} \end{bmatrix}$$

in analogy to (11) and (15).

Since

$$(37) \quad \nu^{kl}(\mathbf{n}) = \nu^{00}(\mathbf{n} - \tau(k, l)), \quad \mu^{kl}(\mathbf{n}) = \mu^{00}(\mathbf{n} - \tau(k, l)),$$

(30) follows from (29) and (25).

By (29) and restricting (25) to $\mathcal{M}_{0j}^{10}, j = 0, 1$, we obtain

$$g_{2j}^{00} = g_{0j}^{10} = e^{i\theta_{10}} e^{-i\psi_{0j}} \odot f_{0j}^{10} = e^{i\theta_{10}} e^{-i\psi_{0j}} \odot f_{2j}^{00}, \quad j = 0, 1,$$

which implies by (25)

$$\begin{aligned}\nu_{2j}^{00} &= e^{i\theta_{00}} e^{-i\theta_{10}} e^{i\psi_{0j}} \odot \mu_{2j}^{00}, \quad j = 0, 1, \\ \nu_{j2}^{00} &= e^{i\theta_{00}} e^{-i\theta_{01}} e^{i\psi_{j0}} \odot \mu_{j2}^{00}, \quad j = 0, 1,\end{aligned}$$

and consequently (31) and (32).

By (37) and restricting (25) to $\mathcal{M}_{2j}^{kl}, \mathcal{M}_{j2}^{kl}, j = 0, 1$, we have (34) and (35).

For (36) with $(k, l) = (0, 0)$, the block $\mathcal{M}_{02}^{10} = \mathcal{M}_{22}^{00}$ is masked by μ_{02}^{10} , a translate of μ_{02}^{00} . By restricting (25) to \mathcal{M}_{02}^{10} ,

$$(38) \quad g_{22}^{00} = g_{02}^{10} = e^{i(\theta_{10} + \theta_{01} - \theta_{00})} e^{-i\psi_{00}} \odot f_{22}^{00}.$$

which is equivalent to (36) with $(k, l) = (0, 0)$. Then (25) and (38) imply

$$(39) \quad \nu_{22}^{00} = e^{i(\theta_{00} - \theta_{10})} e^{i(\theta_{00} - \theta_{01})} e^{i\psi_{00}} \odot \mu_{22}^{00}$$

which is equivalent to (33).

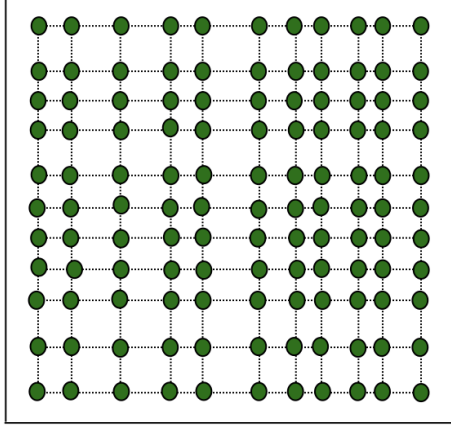
For (36) with general k, l , by restricting (25) to \mathcal{M}_{22}^{kl} and (39) we have

$$g_{22}^{kl} = e^{i\theta_{kl}} e^{i(\theta_{10} - \theta_{00})} e^{i(\theta_{01} - \theta_{00})} e^{-i\psi_{00}} \odot f_{00}^{kl}$$

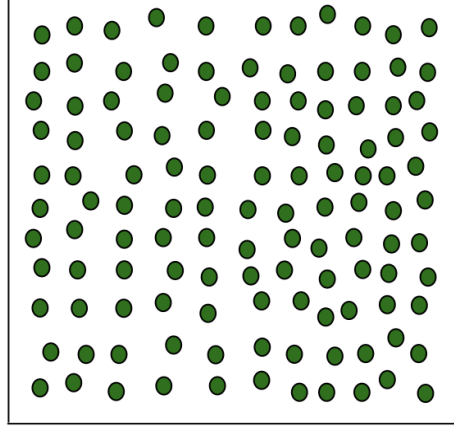
and hence (36). □

When $\tau = 1$, the non-periodic, arithmetically progressing ambiguity and the affine phase ambiguity become the same. In addition, for $\tau = 1$ the raster grid pathology becomes a constant phase factor which can be ignored [17].

Corollary 4.5. *If $\tau = 1$ (i.e. $q = n, p = m$) and (25) holds, then the probe and the object can be uniquely and simultaneously determined.*



(a) Perturbed grid (40)



(b) Perturbed grid (41)

Proof. For $\tau = 1$, μ_{00} consists of just one pixel and ψ is a number. Hence $\mu^{00} = \nu^{00}$ up to a constant phase factor and (27)-(28) then imply that the affine phase ambiguity is the only ambiguity modulo the constant phase factor.

□

5. SLIGHTLY PERTURBED RASTER SCAN

In this section, we demonstrate a simple way for removing all the raster scan ambiguities except for the scaling factor and the affine phase ambiguity.

For the rest of the paper, we assume that f does not vanish in \mathbb{Z}_n^2 .

We consider the perturbed raster scan (Fig. 5(a))

$$(40) \quad \mathbf{t}_{kl} = \tau(k, l) + (\delta_k^1, \delta_l^2), \quad k, l = 0, \dots, q-1$$

where δ_k^1, δ_l^2 are small integers relative to τ and $m - \tau$ (see Theorem 5.5 for details). More general than (40) is the perturbed grid pattern (Fig. 5(b)):

$$(41) \quad \mathbf{t}_{kl} = \tau(k, l) + (\delta_{kl}^1, \delta_{kl}^2), \quad k, l = 0, \dots, q-1,$$

which is harder to analyze and implement in experimental practice (we will only present numerical simulation for it). Without loss of generality we set $\delta_0^1 = \delta_0^2 = 0$ and hence $\mathbf{t}_{00} = (0, 0)$.

Let us express the probe and object errors in terms of

$$(42) \quad \nu^{00}(\mathbf{n})/\mu^{00}(\mathbf{n}) := \alpha(\mathbf{n}) \exp(i\phi(\mathbf{n})), \quad \mathbf{n} \in \mathcal{M}^{00}$$

$$(43) \quad h(\mathbf{n}) := \ln g(\mathbf{n}) - \ln f(\mathbf{n}), \quad \mathbf{n} \in \mathbb{Z}_n^2,$$

where we assume $\alpha(\mathbf{n}) \neq 0$ for all $\mathbf{n} \in \mathcal{M}^{00}$, and rewrite (4) as

$$(44) \quad h(\mathbf{n} + \mathbf{t}) = i\theta_{\mathbf{t}} - \ln \alpha(\mathbf{n}) - i\phi(\mathbf{n}) \pmod{i2\pi},$$

for $\mathbf{n} \in \mathcal{M}^{00}$.

By (44) with $\mathbf{t} = (0, 0)$,

$$(45) \quad h(\mathbf{n}) = i\theta_{00} - \ln \alpha(\mathbf{n}) - i\phi(\mathbf{n}), \quad \forall \mathbf{n} \in \mathcal{M}^{00}$$

and hence for all $\mathbf{t} \in \mathcal{T}$ and $\mathbf{n} \in \mathcal{M}^{00}$

$$(46) \quad h(\mathbf{n} + \mathbf{t}) - h(\mathbf{n}) = i\theta_{\mathbf{t}} - i\theta_{00} \pmod{i2\pi}.$$

We wish to generalize such a relationship to the case where \mathbf{t} in (60) is replaced by $\mathbf{e}_1 = (1, 0)$ and $\mathbf{e}_2 = (0, 1)$.

5.1. A simple perturbation. Let us first study the simple example of the two-shift perturbation to the raster-scan with $\delta_2^1 = \delta_2^2 = -1$ but all other $\delta_k^j = 0$, i.e. $\mathbf{t}_{kl} = \tau(k, l)$ for $(k, l) \neq (2, 0), (0, 2)$. Then

$$(47) \quad h(\mathbf{n} + 2\mathbf{t}_{10} - \mathbf{t}_{20}) = h(\mathbf{n} + (1, 0))$$

$$(48) \quad h(\mathbf{n} + 2\mathbf{t}_{01} - \mathbf{t}_{02}) = h(\mathbf{n} + (0, 1)).$$

There are several routes of reduction from $(1, 0)$ to $(0, 0)$ via the shifts in \mathcal{T} . For example, we can proceed from $(1, 0) = 2\mathbf{t}_{10} - \mathbf{t}_{20}$ to $(0, 0)$ along the path

$$(49) \quad (2\mathbf{t}_{10} - \mathbf{t}_{20}) \longrightarrow (\mathbf{t}_{10} - \mathbf{t}_{20}) \longrightarrow \mathbf{t}_{10} \longrightarrow (0, 0)$$

by repeatedly applying (46) where the direction of the second step is to be reversed since $-\mathbf{t}_{20} \notin \mathcal{T}$ (\mathcal{T} is no longer a group even under the periodic boundary condition). The direction is important for keeping track of the domain of validity of (46) along the path. Hence for all

$$(50) \quad \mathbf{n} \in (\mathcal{M}^{00} + \mathbf{t}_{20} - \mathbf{t}_{10}) \cap \mathcal{M}^{00}$$

we have

$$\begin{aligned} h(\mathbf{n} + 2\mathbf{t}_{10} - \mathbf{t}_{20}) &= h(\mathbf{n} + \mathbf{t}_{10} - \mathbf{t}_{20}) + i\theta_{10} - i\theta_{00} \\ &= h(\mathbf{n} + \mathbf{t}_{10}) + i\theta_{10} - i\theta_{20} \\ &= h(\mathbf{n}) + 2i\theta_{10} - i\theta_{20} - i\theta_{00} \end{aligned}$$

and hence

$$(51) \quad h(\mathbf{n} + (1, 0)) = h(\mathbf{n}) + i\Delta^1, \quad \Delta^1 := 2\theta_{10} - \theta_{20} - \theta_{00}$$

modulo $i2\pi$.

Let us consider another alternative route for reduction:

$$(52) \quad (2\mathbf{t}_{10} - \mathbf{t}_{20}) \longrightarrow 2\mathbf{t}_{10} \longrightarrow \mathbf{t}_{10} \longrightarrow (0, 0)$$

where the proper direction for the first step in applying (46) is reversed. Keeping track of the domain of validity along the path, we have

$$\begin{aligned} h(\mathbf{n} + 2\mathbf{t}_{10} - \mathbf{t}_{20}) &= h(\mathbf{n} + 2\mathbf{t}_{10}) - i\theta_{20} + i\theta_{00} \\ &= h(\mathbf{n} + \mathbf{t}_{10}) + i\theta_{10} - i\theta_{20} \\ &= h(\mathbf{n}) + i\Delta^1 \end{aligned}$$

for all

$$(53) \quad \mathbf{n} \in (\mathcal{M}^{00} - 2\mathbf{t}_{10} + \mathbf{t}_{20}) \cap (\mathcal{M}^{00} - \mathbf{t}_{10}) \cap \mathcal{M}^{00}.$$

In summary, (51) holds for all \mathbf{n} in the union of (50) and (53), i.e.

$$D^1 = ([0, m - \tau - 1] \cup [\tau - 1, m - 1]) \times [0, m - 1].$$

Clearly including other routes for reducing $2\mathbf{t}_{10} - \mathbf{t}_{20}$ to $(1, 0)$ in D^1 can enlarge the domain of validity for (51). For simplicity of argument, we omit them here.

By repeatedly applying (46) we have the following result.

Proposition 5.1. *The relation (51) holds true in the set*

$$(54) \quad \bigcup_{\mathbf{t} \in \mathcal{T}} [\mathbf{t} + D^1 \cap \mathcal{M}^{00} \cap (\mathcal{M}^{00} - \mathbf{e}_1)]$$

which contains \mathbb{Z}_n^2 if

$$(55) \quad \tau \leq (m - 2) \wedge [(m + 1)/2].$$

Proof. For $\mathbf{n} \in D^1 \cap \mathcal{M}^{00} \cap (\mathcal{M}^{00} - \mathbf{e}_1)$, we have

$$(56) \quad h(\mathbf{n} + \mathbf{t}) = h(\mathbf{n} + \mathbf{e}_1) - i\Delta^1 + i\theta_{\mathbf{t}} - i\theta_{00},$$

by (51) and (46).

Hence, by (46) and (56),

$$\begin{aligned} h(\mathbf{n} + \mathbf{e}_1 + \mathbf{t}) &= h(\mathbf{n} + \mathbf{e}_1) + i\theta_{\mathbf{t}} - i\theta_{00} \\ &= h(\mathbf{n} + \mathbf{t}) + i\Delta^1. \end{aligned}$$

In other words, (51) has been extended to $\mathbf{t} + D^1 \cap \mathcal{M}^{00} \cap (\mathcal{M}^{00} - \mathbf{e}_1)$. Taking the union over all shifts, we obtain (54).

For the second part of the proposition, let us write the set (54) explicitly as

$$\bigcup_{k,l=0}^{q-1} \{ \tau(k, l) + ([0, m - \tau - 1] \cup [\tau - 1, m - 1]) \cap [0, m - 2] \} \times [0, m - 1].$$

Note that

$$\begin{aligned} ([0, m - \tau - 1] \cup [\tau - 1, m - 1]) \cap [0, m - 2] &= [0, m - \tau - 1] \cup [\tau - 1, m - 2] \\ &= [0, m - 2] \end{aligned}$$

under $m - \tau - 1 \geq \tau - 2$ or, equivalently, (55). To complete the argument, observe that the adjacent rectangles among

$$(\tau(k, l) + [0, m - 2]) \times [0, m - 1], \quad k, l = 0, \dots, q - 1,$$

have zero gap if $\tau \leq m - 2$.

□

By the same argument under (55), it follows from (48) that for all $\mathbf{n} \in \mathbb{Z}_n^2$

$$(57) \quad h(\mathbf{n} + (0, 1)) = h(\mathbf{n}) + i\Delta^2 \pmod{2\pi}, \quad \Delta^2 := 2i\theta_{01} - i\theta_{02} - i\theta_{00}.$$

In conclusion,

$$(58) \quad h(\mathbf{n}) = h(0) + i\mathbf{n} \cdot \mathbf{r} \pmod{2\pi}, \quad \forall \mathbf{n} \in \mathbb{Z}_n^2,$$

where $\mathbf{r} = (\Delta^1, \Delta^2)$.

5.2. General perturbation. Next we consider more general perturbations $\{\delta_k^i\}$ to the raster scan and derive (58).

Let us rewrite (46) in a different form: Subtracting the respective (46) for \mathbf{t} and \mathbf{t}' , we obtain the equivalent form

$$(59) \quad h(\mathbf{n} + \mathbf{t}) - h(\mathbf{n} + \mathbf{t}') = i\theta_{\mathbf{t}} - i\theta_{\mathbf{t}'} \pmod{i2\pi},$$

for any $\mathbf{n} \in \mathcal{M}^{00}$ and $\mathbf{t}, \mathbf{t}' \in \mathcal{T}$, which can also be written as

$$(60) \quad h(\mathbf{n} + \mathbf{t} - \mathbf{t}') = h(\mathbf{n}) + i(\theta_{\mathbf{t}} - \theta_{\mathbf{t}'}) \pmod{i2\pi},$$

for $\mathbf{n} \in \mathcal{M}^{\mathbf{t}'}$ by shifting the argument of h .

Consider the triplets of shifts

$$(\mathbf{t}_{kl}, \mathbf{t}_{k+1,l}, \mathbf{t}_{k+2,l}), \quad (\mathbf{t}_{kl}, \mathbf{t}_{k,l+1}, \mathbf{t}_{k,l+2})$$

for which we have

$$\begin{aligned} 2(\mathbf{t}_{k+1,l} - \mathbf{t}_{kl}) - (\mathbf{t}_{k+2,l} - \mathbf{t}_{kl}) &= (2\delta_{k+1}^1 - \delta_k^1 - \delta_{k+2}^1, 0) := (a_k^1, 0), \\ 2(\mathbf{t}_{k,l+1} - \mathbf{t}_{kl}) - (\mathbf{t}_{k,l+2} - \mathbf{t}_{kl}) &= (0, 2\delta_{l+1}^2 - \delta_l^2 - \delta_{l+2}^2) := (0, a_l^2). \end{aligned}$$

Analogous to (52) and (49) the paths of reduction

$$(2\mathbf{t}_{k+1,l} - \mathbf{t}_{kl} - \mathbf{t}_{k+2,l}) \longrightarrow 2(\mathbf{t}_{k+1,l} - \mathbf{t}_{kl}) \longrightarrow (\mathbf{t}_{k+1,l} - \mathbf{t}_{kl}) \longrightarrow (0, 0)$$

and

$$(2\mathbf{t}_{k+1,l} - \mathbf{t}_{kl} - \mathbf{t}_{k+2,l}) \longrightarrow (\mathbf{t}_{k+1,l} - \mathbf{t}_{k+2,l}) \longrightarrow (\mathbf{t}_{k+1,l} - \mathbf{t}_{kl}) \longrightarrow (0, 0)$$

lead to

$$(61) \quad h(\mathbf{n} + (a_k^1, 0)) = h(\mathbf{n}) + 2i\theta_{k+1,l} - i\theta_{k+2,l} - i\theta_{kl} \pmod{i2\pi}$$

for all $\mathbf{n} \in D_{kl}^1$ where

$$\begin{aligned} D_{kl}^1 &:= \{ \mathcal{M}^{kl} \cap [\mathcal{M}^{kl} - 2\mathbf{t}_{k+1,l} + \mathbf{t}_{k+2,l} + \mathbf{t}_{kl}] \cap [\mathcal{M}^{kl} - \mathbf{t}_{k+1,l} + \mathbf{t}_{kl}] \} \\ &\quad \bigcup \{ \mathcal{M}^{kl} \cap [\mathcal{M}^{kl} + \mathbf{t}_{k+2,l} - \mathbf{t}_{k+1,l}] \} \\ &= \{ \mathcal{M}^{kl} \cap [\mathcal{M}^{kl} - (a_k^1, 0)] \cap [\mathcal{M}^{kl} - (\tau + \delta_{k+1}^1 - \delta_k^1, 0)] \} \\ &\quad \bigcup \{ \mathcal{M}^{kl} \cap [\mathcal{M}^{kl} + (\tau + \delta_{k+2}^1 - \delta_{k+1}^1, 0)] \} \end{aligned}$$

Likewise, repeatedly applying (60) along the paths,

$$(2\mathbf{t}_{k,l+1} - \mathbf{t}_{kl} - \mathbf{t}_{k,l+2}) \longrightarrow 2(\mathbf{t}_{k,l+1} - \mathbf{t}_{kl}) \longrightarrow (\mathbf{t}_{k,l+1} - \mathbf{t}_{kl}) \longrightarrow (0, 0)$$

and

$$(2\mathbf{t}_{k,l+1} - \mathbf{t}_{kl} - \mathbf{t}_{k+2,l}) \longrightarrow (\mathbf{t}_{k+1,l} - \mathbf{t}_{k+2,l}) \longrightarrow (\mathbf{t}_{k+1,l} - \mathbf{t}_{kl}) \longrightarrow (0, 0)$$

we get

$$(62) \quad h(\mathbf{n} + (0, a_l^2)) = h(\mathbf{n}) + 2i\theta_{k,l+1} - i\theta_{k,l+2} - i\theta_{kl} \pmod{i2\pi}$$

for $\mathbf{n} \in D_{kl}^2$ where

$$\begin{aligned} D_{kl}^2 &:= \{ \mathcal{M}^{kl} \cap [\mathcal{M}^{kl} - 2\mathbf{t}_{k,l+1} + \mathbf{t}_{k,l+2} + \mathbf{t}_{kl}] \cap [\mathcal{M}^{kl} - \mathbf{t}_{k,l+1} + \mathbf{t}_{kl}] \} \\ &\quad \bigcup \{ \mathcal{M}^{kl} \cap [\mathcal{M}^{kl} + \mathbf{t}_{k,l+2} - \mathbf{t}_{k,l+1}] \} \\ &= \{ \mathcal{M}^{kl} \cap [\mathcal{M}^{kl} - (0, a_l^2)] \cap [\mathcal{M}^{kl} - (0, \tau + \delta_{l+1}^2 - \delta_l^2)] \} \\ &\quad \bigcup \{ \mathcal{M}^{kl} \cap [\mathcal{M}^{kl} + (0, \tau + \delta_{l+2}^2 - \delta_{l+1}^2)] \}. \end{aligned}$$

Lemma 5.2. *Let k, l be fixed. The relations (61) and (62) hold true in the sets*

$$(63) \quad \bigcup_{\mathbf{t} \in \mathcal{T}} [\mathbf{t} + D_{kl}^1 \cap \mathcal{M}^{kl} \cap (\mathcal{M}^{kl} - (a_k^1, 0))] \quad \text{and}$$

$$(64) \quad \bigcup_{\mathbf{t} \in \mathcal{T}} [\mathbf{t} + D_{kl}^2 \cap \mathcal{M}^{kl} \cap (\mathcal{M}^{kl} - (0, a_l^2))] ,$$

respectively. Both sets contain \mathbb{Z}_n^2 if the following conditions hold:

$$(65) \quad \max_{i=1,2} \{ |a_k^i| + \delta_{k+1}^i - \delta_k^i \} \leq \tau$$

$$(66) \quad 2\tau \leq m - \max_{i=1,2} \{ \delta_{k+2}^i - \delta_k^i \}$$

$$(67) \quad \max_{k'} \max_{i=1,2} \{ |a_k^i| + \delta_{k'+1}^i - \delta_{k'}^i \} \leq m - 1 - \tau.$$

Remark 5.3. *Proposition 5.1 corresponds to $(k, l) = (0, 0)$ with (65), (66) and (67) reduced to*

$$1 \leq \tau, \quad 2\tau \leq m + 1, \quad \tau \leq m - 2,$$

respectively.

Remark 5.4. *Inequalities (65) and (67) are smallness conditions for the perturbations relative to the average step size and the overlap between the adjacent probes. The most consequential condition (66) suggests an average overlap ratio of at least 50%, i.e. under-shifted raster scan.*

Proof. The argument follows the same pattern as that for Proposition 5.1.

For $\mathbf{n} \in D_{kl}^1 \cap \mathcal{M}^{00} \cap (\mathcal{M}^{00} - (a_k^1, 0))$, we have

$$h(\mathbf{n} + \mathbf{t}) = h(\mathbf{n} + (a_k^1, 0)) - i(2\theta_{k+1,l} - \theta_{k+2,l} - \theta_{kl}) + i\theta_{\mathbf{t}} - i\theta_{00}$$

by (61) and (46).

Hence, by (46) and (56),

$$\begin{aligned} h(\mathbf{n} + (a_k^1, 0) + \mathbf{t}) &= h(\mathbf{n} + (a_k^1, 0)) + i\theta_{\mathbf{t}} - i\theta_{00} \\ &= h(\mathbf{n} + \mathbf{t}) + i(2\theta_{k+1,l} - \theta_{k+2,l} - \theta_{kl}). \end{aligned}$$

Taking the union over all shifts, we obtain the set in (63). The case for (64) is similar.

For the second part of the proposition, note that

$$(68) \quad \mathcal{M}^{kl} \cap (\mathcal{M}^{kl} - (a_k^1, 0)) = \llbracket 0, m-1 - |a_k^1| \rrbracket \times \llbracket 0, m-1 \rrbracket \quad \text{if } a_k^1 \geq 0 \\ \text{or } \llbracket |a_k^1|, m-1 \rrbracket \times \llbracket 0, m-1 \rrbracket, \quad \text{if } a_k^1 < 0.$$

In the former case in (68) the set (63) contains

$$(69) \quad \bigcup_{\mathbf{t} \in \mathcal{T}} [\mathbf{t} + \mathbf{t}_{kl} + (\llbracket 0, m-1 - \tau - \delta_{k+1}^1 + \delta_k^1 \rrbracket \cup \llbracket \tau + \delta_{k+2}^1 - \delta_{k+1}^1, m-1 \rrbracket) \\ \times \llbracket 0, m-1 \rrbracket \cap (\llbracket 0, m-1 - |a_k^1| \rrbracket \times \llbracket 0, m-1 \rrbracket)]$$

under the condition

$$(70) \quad |a_k^1| + \delta_{k+1}^1 - \delta_k^1 \leq \tau \leq m-1 - |a_k^1| - \delta_{k+1}^1 + \delta_k^1.$$

The set in (69) becomes

$$(71) \quad \bigcup_{\mathbf{t} \in \mathcal{T}} [\mathbf{t} + \mathbf{t}_{kl} + (\llbracket 0, m-1 \rrbracket \cap \llbracket 0, m-1 - |a_k^1| \rrbracket) \times \llbracket 0, m-1 \rrbracket] \\ = \bigcup_{\mathbf{t} \in \mathcal{T}} [\mathbf{t} + \mathbf{t}_{kl} + \llbracket 0, m-1 - |a_k^1| \rrbracket \times \llbracket 0, m-1 \rrbracket]$$

under the condition

$$(72) \quad m-1 - \tau - \delta_{k+1}^1 + \delta_k^1 \geq \tau + \delta_{k+2}^1 - \delta_{k+1}^1 - 1.$$

The set in (71) contains \mathbb{Z}_n^2 if for each l' the adjacent sets among

$$\tau(k' + k, l' + l) + (\delta_{k'}^1 + \delta_k^1, \delta_{l'}^2 + \delta_l^2) + \llbracket 0, m-1 - |a_k^1| \rrbracket \times \llbracket 0, m-1 \rrbracket,$$

for $k' = 0, \dots, q-1$, have no gap between them, which is the case if

$$(73) \quad \tau + \delta_{k'+1}^1 - \delta_{k'}^1 \leq m-1 - |a_k^1|, \quad \forall k'.$$

Note that (73) subsumes the second inequality in (70).

Likewise for the latter case in (68) the set in (63) contains

$$(74) \quad \bigcup_{\mathbf{t} \in \mathcal{T}} [\mathbf{t} + \mathbf{t}_{kl} + (\llbracket |a_k^1|, m-1 - \tau - \delta_{k+1}^1 + \delta_k^1 \rrbracket \cup \llbracket \tau + \delta_{k+2}^1 - \delta_{k+1}^1, m-1 \rrbracket) \\ \times \llbracket 0, m-1 \rrbracket \cap (\llbracket |a_k^1|, m-1 \rrbracket \times \llbracket 0, m-1 \rrbracket)]$$

under the condition

$$(75) \quad |a_l^2| + \delta_{l+1}^2 - \delta_l^2 \leq \tau \leq m-1 - |a_l^2| - \delta_{l+1}^2 + \delta_l^2.$$

The set in (74) in turn becomes

$$\bigcup_{\mathbf{t} \in \mathcal{T}} [\mathbf{t} + \mathbf{t}_{kl} + \llbracket |a_k^1|, m-1 \rrbracket \times \llbracket 0, m-1 \rrbracket]$$

under the condition

$$m-1 - \tau - \delta_{k+1}^1 + \delta_k^1 \geq \tau + \delta_{k+2}^1 - \delta_{k+1}^1 - 1.$$

The set in (76) contains \mathbb{Z}_n^2 if for each l' the adjacent sets among

$$\tau(k' + k, l' + l) + (\delta_{k'}^1 + \delta_k^1, \delta_{l'}^2 + \delta_l^2) + \llbracket |a_k^1|, m-1 \rrbracket \times \llbracket 0, m-1 \rrbracket,$$

for $k' = 0, \dots, q-1$, have no gap between them, which is the case under the same condition (73) which subsumes the second inequality in (75).

The case with (64) can be proved by the same argument as above. \square

Since \mathcal{M}^{kl} overlaps with $\mathcal{M}^{k+1,l}$ and $\mathcal{M}^{k,l+1}$ which in turn overlap with $\mathcal{M}^{k+2,l}$ and $\mathcal{M}^{k,l+2}$, respectively (and so on), the quantities

$$(76) \quad \Delta_k^1 := 2\theta_{k+1,l} - \theta_{k+2,l} - \theta_{kl}$$

$$(77) \quad \Delta_l^2 := 2\theta_{k,l+1} - \theta_{k,l+2} - \theta_{kl}$$

on the righthand side of (61) and (62) depend only on one index and we can write

Suppose further that there exist $c_k^1, c_l^2 \in \mathbb{Z}$ such that

$$(78) \quad \sum_{k=0}^{q-1} c_k^1 a_k^1 = \sum_{l=0}^{q-1} c_l^2 a_l^2 = 1,$$

i.e. $\{a_i^j\}$ are co-prime integers for each $j = 1, 2$.

Then by repeatedly using (61)-(62) we arrive at

$$\begin{aligned} h(\mathbf{n} + (1, 0)) &= h\left(\mathbf{n} + \left(\sum_k c_k^1 a_k^1, 0\right)\right) = h(\mathbf{n}) + ir_1 \pmod{i2\pi} \\ h(\mathbf{n} + (0, 1)) &= h\left(\mathbf{n} + \left(0, \sum_l c_l^2 a_l^2\right)\right) = h(\mathbf{n}) + ir_2 \pmod{i2\pi} \end{aligned}$$

where

$$(79) \quad r_1 = \sum_{k=0}^{q-1} c_k^1 \Delta_k^1, \quad r_2 = \sum_{l=0}^{q-1} c_l^2 \Delta_l^2.$$

Therefore, we obtain (58) with $\mathbf{r} = (r_1, r_2)$ given by (79). Following through the rest of argument we can prove the following result.

Theorem 5.5. *Suppose f does not vanish in \mathbb{Z}_n^2 . For the perturbed raster scan (40), let $\{\delta_{j_k}^i\}$ be the subset of perturbations satisfying*

$$(80) \quad \tau \geq \max_{i=1,2} \{|a_{j_k}^i| + \delta_{j_k+1}^i - \delta_{j_k}^i\}$$

$$(81) \quad 2\tau \leq m - \max_{i=1,2} \{\delta_{j_k+2}^i - \delta_{j_k}^i\}$$

$$(82) \quad m - \tau \geq 1 + \max_{k'} \max_{i=1,2} \{|a_{j_k}^i| + \delta_{k'+1}^i - \delta_{k'}^i\}$$

where $a_j^i = 2\delta_{j+1}^i - \delta_j^i - \delta_{j+2}^i$. Suppose

$$(83) \quad \gcd(|a_{j_k}^i|) = 1, \quad i = 1, 2.$$

Let $\mathbf{r} = (r_1, r_2) \in \mathbb{R}^2$ be given by (79) and $\{c_i^j\}$ be any solution to (78) such that $\{c_{j_k}^i\}$ are the only nonzero entries.

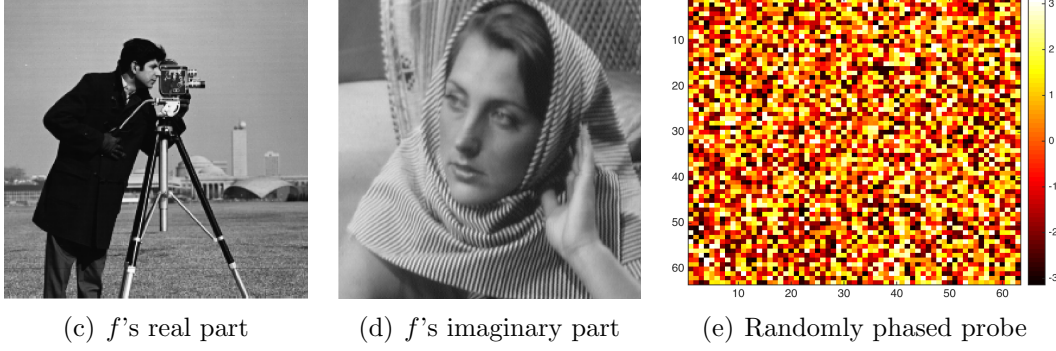


FIGURE 2. The real part (a) and the imaginary part (b) of the object and (c) randomly phased probe μ^{00} .

Then both the object and probe errors have a constant scaling factor and an affine phase profile:

$$(84) \quad g(\mathbf{n})/f(\mathbf{n}) = \alpha^{-1}(0) \exp(\mathbf{i}\mathbf{n} \cdot \mathbf{r}),$$

$$(85) \quad \nu^0(\mathbf{n})/\mu^0(\mathbf{n}) = \alpha(0) \exp(\mathbf{i}\phi(0) - \mathbf{i}\mathbf{n} \cdot \mathbf{r}).$$

Further the block phases have an affine profile:

$$(86) \quad \theta_{kl} = \theta_{00} + \mathbf{t}_{kl} \cdot \mathbf{r} \mod 2\pi,$$

for $k, l = 0, \dots, q-1$.

Remark 5.6. It can be verified through a tedious calculation that (86) (with (76)-(77), (78) and (79)) is an underdetermined linear system for $\{\theta_{kl}\}$, which is consistent with the fact that the affine phase ambiguity (1)-(2) is inherent to any blind ptychography.

Proof. It remains to verify (85) and (85) which follow immediately from (44) and (84).

The block phase relation (86) follows upon substituting $\mathbf{t} = \mathbf{t}_{kl}$ and (84) into (44).

To summarize, we have shown that the scaling factor in (85) and the affine phase ambiguity, in (84) and (85), are the only ambiguities for the slightly perturbed raster scan (40).

□

6. NUMERICAL EXPERIMENTS

In this section we demonstrate geometric convergence for blind ptychography with the perturbed raster scan (40).

Let $\mathcal{F}(\nu, g) \in \mathbb{C}^N$ be the totality of the Fourier (magnitude and phase) data corresponding to the probe ν and the object g such that $|\mathcal{F}(\mu, f)| = b$ where b is the noiseless ptychographic data. Since $\mathcal{F}(\cdot, \cdot)$ is a bilinear function, $A_k h := \mathcal{F}(\mu_k, h)$, $k \geq 1$, defines a matrix A_k for the k -th probe estimate μ_k and $B_k \eta := \mathcal{F}(\eta, f_{k+1})$, $k \geq 1$, for the $(k+1)$ -st image estimate f_{k+1} such that $A_k f_{j+1} = B_j \mu_k$, $j \geq 1, k \geq 1$. Let $P_k = A_k A_k^\dagger$ be the orthogonal projection onto

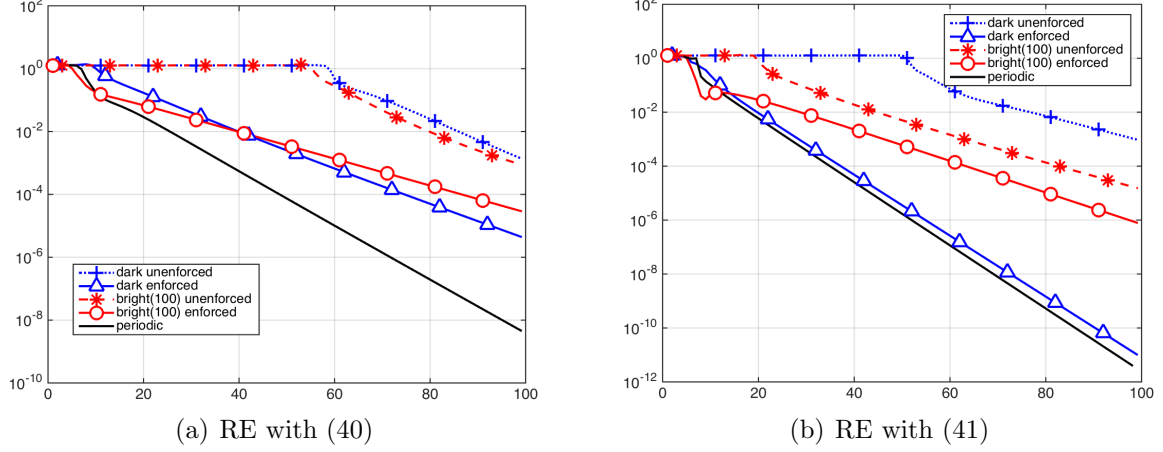


FIGURE 3. RE for various boundary conditions with the sampling scheme (a) (40) and (b) (41).

the range of A_k and $R_k = 2P_k - I$ the corresponding reflector. Likewise, let $Q_k = B_k B_k^\dagger$ be the orthogonal projection onto the range of B_k and S_k the corresponding reflector.

Algorithm 1: Alternating minimization (AM)

- 1: Input: initial probe guess μ_1 .
 - 2: Update the object estimate $f_{k+1} = \arg \min \mathcal{L}(A_k g)$ s.t. $g \in \mathbb{C}^{n \times n}$.
 - 3: Update the probe estimate $\mu_{k+1} = \arg \min \mathcal{L}(B_k \nu)$ s.t. $\nu \in \mathbb{C}^{m \times m}$.
 - 4: Terminate if $\|B_k \mu_{k+1} - b\|_2$ stagnates or is less than tolerance; otherwise, go back to step 2 with $k \rightarrow k + 1$.
-

We use the objective function

$$\mathcal{L}(y) = \frac{1}{2} \| |y| - b \|_2^2$$

and a randomly chosen initial probe guess satisfying

$$\Re [\overline{\mu_1}(\mathbf{n}) \odot \mu^{00}(\mathbf{n})] > 0, \quad \forall \mathbf{n},$$

i.e. each pixel of the probe guess is aligned with the corresponding pixel of the true probe positively. The inner loops for updating the object and probe estimates are carried out by the Douglas-Rachford splitting method as detailed in [3, 11]: At epoch k , for $l = 1, 2, 3, \dots$

$$\begin{aligned} u_k^{l+1} &= \frac{1}{2} u_k^l + \frac{1}{2} b \odot \text{sgn}(R_k u_k^l), & u_k^1 &= u_{k-1}^\infty \\ v_k^{l+1} &= \frac{1}{2} v_k^l + \frac{1}{2} b \odot \text{sgn}(S_k v_k^l), & v_k^1 &= v_{k-1}^\infty \end{aligned}$$

with the object estimate $f_{k+1} = A_k^\dagger u_k^\infty$ and the probe estimate $\mu_{k+1} = B_k^\dagger v_k^\infty$ where u_k^∞ and v_k^∞ are terminal values of the k -th epoch of the inner loops. In the simulation for Fig. 3 we keep the maximum number of iterations in the inner loop to 30.

To discount the constant amplitude offset and the linear phase ambiguity we consider the following relative error (RE) for the recovered image f_k and probe μ_k at the k^{th} epoch:

$$(87) \quad \text{RE}(k) = \min_{\alpha \in \mathbb{C}, \mathbf{k} \in \mathbb{R}^2} \frac{\|f(\mathbf{k}) - \alpha e^{-i2\pi \mathbf{k} \cdot \mathbf{r}/n} f_k(\mathbf{k})\|_2}{\|f\|_2}$$

The image is 256-by-256 Cameraman+ i Barbara (CiB). We use the randomly phased probe $\mu^{00}(\mathbf{n}) = \exp[i\phi(\mathbf{n})]$ where $[\phi(\mathbf{n})]$ are 60×60 i.i.d. uniform random variables over $[0, 2\pi)$. We let δ_k^1 (resp. δ_{kl}^1) and δ_l^2 (resp. δ_{kl}^2) to be i.i.d. uniform random variables over $[-4, 4]$. In other words, the adjacent probes overlap by an average of $1 - \tau/m = 50\%$.

When the probe steps outside of the boundary of the object domain, the area $\mathcal{M} \setminus \mathbb{Z}_n^2$ needs special treatment in the reconstruction process.

The periodic boundary condition forces the slope \mathbf{r} in the linear phase ambiguity to be integers. The dark-field and bright-field boundary conditions assume zero and nonzero ($= 100$ in the simulation) values, respectively, in $\mathcal{M} \setminus \mathbb{Z}_n^2$. When the bright-field boundary condition is present in the simulation data and enforced in reconstruction, the linear phase ambiguity disappears from the object estimate. On the contrary, enforcing the dark-field boundary condition can not remove the linear phase ambiguity. In both cases, however, enforcement of boundary condition in reconstruction speeds up the convergence as shown in Figure 3.

Figure 3 shows that the sampling scheme (41) generally outperforms (40) with a faster convergence rate, indicating that higher level of disorder in the grid pattern is better for blind ptychography.

7. CONCLUSIONS

We have studied the artifacts in blind ptychographic reconstruction from the perspective of uniqueness theory of inverse problems and identified the periodic ambiguities in the raster scan ptychography as the raster grid pathology reported in the optics literature.

We have given a complete characterization of blind ptychographic ambiguities for the raster scan including the periodic and non-periodic ambiguities. The non-periodic ambiguity have an affine profile mirroring that of the block phases. To the best of our knowledge, such an ambiguity has not been reported in the literature.

We have presented a slightly perturbed under-shifted raster scan and proved that such a scheme can remove all the ambiguities except for those inherent to any blind ptychography, namely the scaling factor and the affine phase ambiguity. In comparison, the same goal is approached in [1] not by changing the raster scan but by considering only a set of generic objects.

For the perturbed under-shifted raster scan (40) with small random δ_j^i , it is highly probable that the co-prime condition (83) holds for large q and hence only the scaling factor and the affine phase ambiguity are present under (65)-(67) [19]. It would be interesting to see if the analysis presented in Section 5 can be extended to other scan patterns in practice

such as the concentric circles [6, 36, 37], the Fermat spiral [13] and those designed for Fourier ptychography [13].

In a noisy ptychographic experiment with the raster scan, as the step size shrinks, raster grid pathology becomes less apparent and eventually invisible before the step size reaches 1 [14] (cf. Corollary 4.5). The affine phase ambiguity and the raster grid pathology can also be suppressed by additional prior information such as the Fourier intensities of the probe [23].

ACKNOWLEDGMENT

This work was supported by the National Science Foundation under Grant DMS-1413373. I thank National Center for Theoretical Sciences (NCTS), Taiwan, where the present work was completed, for the hospitality during my visits in June and August 2018. I am grateful for Zhiqing Zhang for preparing Fig. 3.

REFERENCES

- [1] T. Bendory, D. Edidin and Y. C. Eldar, “Blind phaseless short-time Fourier transform recovery,” arXiv:1808.07414.
- [2] O. Bunk, M. Dierolf, S. Kynde, I. Johnson, O. Marti, F. Pfeiffer, “Influence of the overlap parameter on the convergence of the ptychographical iterative engine,” *Ultramicroscopy* **108** (5) (2008) 481-487.
- [3] P. Chen and A. Fannjiang, “Coded-aperture ptychography: uniqueness and reconstruction”, *Inverse Problems* **34** (2018) 025003.
- [4] H.H. Conway & N.J.A. Sloane, *Sphere Packings, Lattices and Groups*, 3rd ed., Berlin, New York: Springer-Verlag, 1999.
- [5] M. Dierolf, A. Menzel, P. Thibault, P. Schneider, C. M. Kewish, R. Wepf, O. Bunk, and F. Pfeiffer, “Ptychographic x-ray computed tomography at the nanoscale,” *Nature* **467** (2010), 436-439.
- [6] M. Dierolf, P. Thibault, A. Menzel, C. Kewish, K. Jefimovs, I. Schlichting, K. Kong, O. Bunk, and F. Pfeiffer, “Ptychographic coherent diffractive imaging of weakly scattering specimens,” *New J. Phys.* **12** (2010), 035017.
- [7] C. Falldorf, M. Agour, C. V. Kopylow and R. B. Bergmann, “Phase retrieval by means of a spatial light modulator in the Fourier domain of an imaging system,” *Appl. Opt.* **49**, 1826-1830 (2010).
- [8] R. Egami, R. Horisaki, L. Tian & J. Tanida, “Relaxation of mask design for single-shot phase imaging with a coded aperture,” *Appl. Opt.* **55** (2016) 1830-1837.
- [9] A. Fannjiang and P. Chen, “Blind ptychography: uniqueness & ambiguities,” arXiv:1806.02674.
- [10] A. Fannjiang and W. Liao, “Phase retrieval with random phase illumination,” *J. Opt. Soc. A* **29**, 1847-1859 (2012).
- [11] A. Fannjiang and Z. Zhang, “Blind ptychography by Douglas-Rachford splitting,” arXiv:1809.00962.
- [12] M. Guizar-Sicairos, A. Diaz, M. Holler, M. S. Lucas, A. Menzel, R. A. Wepf, and O. Bunk, “Phase tomography from x-ray coherent diffractive imaging projections,” *Opt. Exp.* **19** (2011), 21345-21357.
- [13] K. Guo, S. Dong, P. Nanda and G. Zheng, “Optimization of sampling pattern and the design of Fourier ptychographic illuminator,” *Opt. Exp.* **23** (2015) 6171-6180.
- [14] X. Huang, H. Yan, M. Ge, H. Öztörk, E. Nazaretski, I. K. Robinson and Y.S. Chu, “Artifact mitigation of ptychography integrated with on-the-fly scanning probe microscopy,” *Appl. Phys. Lett.* **111**(2017) 023103.
- [15] X. Huang, H. Yang, R. Harder, Y. Hwu, I.K. Robinson & Y.S. Chu, “Optimization of overlap uniformness for ptychography,” *Opt. Express* **22** (2014), 12634-12644.
- [16] R. Horisaki, R. Egami & J. Tanida, “Single-shot phase imaging with randomized light (SPIRAL).” *Opt. Express* **24**, 3765-3773 (2016).

- [17] M. A. Iwen, A. Viswanathan, and Y. Wang, "Fast phase retrieval from local correlation measurements," *SIAM J. Imaging Sci.* **9**(4)(2016), pp. 1655-1688.
- [18] Y. Jiang, Z. Chen, Y. Han, P. Deb, H. Gao, S. Xie, P. Purohit, M. W. Tate, J. Park, S. M. Gruner, V. Elser & D. A. Muller "Electron ptychography of 2D materials to deep sub-angstrom resolution," *Nature* **559** 343-349 (2018).
- [19] A. M. Maiden, M. J. Humphry, F. Zhang and J. M. Rodenburg, "Superresolution imaging via ptychography," *J. Opt. Soc. Am. A* **28** (2011), 604-612.
- [20] A. Maiden, D. Johnson and P. Li, "Further improvements to the ptychographical iterative engine," *Optica* **4** (2017), 736-745.
- [21] A.M. Maiden, G.R. Morrison, B. Kaulich, A. Gianoncelli & J.M. Rodenburg, "Soft X-ray spectromicroscopy using ptychography with randomly phased illumination," *Nat. Commun.* **4** (2013), 1669.
- [22] A.M. Maiden & J.M. Rodenburg, "An improved ptychographical phase retrieval algorithm for diffractive imaging," *Ultramicroscopy* **109** (2009), 1256-1262.
- [23] S. Marchesini, H. Krishnan, B. J. Daurer, D.A. Shapiro, T. Perciano, J. A. Sethian and F.R.N.C. Maia, "SHARP: a distributed GPU-based ptychographic solver," *J. Appl. Cryst.***49** (2016), 1245-1252.
- [24] Y. S. G. Nashed, D. J. Vine, T. Peterka, J. Deng, R. Ross and C. Jacobsen, "Parallel ptychographic reconstruction," *Opt. Express* **22** (2014) 32082-32097.
- [25] P.D. Nellist, B.C. McCallum & J.M. Rodenburg, "Resolution beyond the information limit in transmission electron microscopy, " *Nature* **374** (1995) 630-632.
- [26] P.D. Nellist and J.M. Rodenburg, " Electron ptychography. I. Experimental demonstration beyond the conventional resolution limits," *Acta Cryst. A* **54** (1998), 49-60.
- [27] K.A. Nugent, "Coherent methods in the X-ray sciences, " *Adv. Phys.* **59** (2010) 1-99.
- [28] X. Ou, G. Zheng and C. Yang, "Embedded pupil function recovery for Fourier ptychographic microscopy," *Opt. Exp.* **22** (2014) 4960-4972.
- [29] X. Peng, G.J. Ruane, M.B. Quadrelli & G.A. Swartzlander, " Randomized apertures: high resolution imaging in far field," *Opt. Express* **25** (2017) 296187.
- [30] F. Pfeiffer, "X-ray ptychography," *Nat. Photon.* **12** (2017) 9-17.
- [31] J.M. Rodenburg, "Ptychography and related diffractive imaging methods," *Adv. Imaging Electron Phys.* **150** (2008) 87-184.
- [32] M.H. Seaberg, A. d'Aspremont & J.J. Turner, "Coherent diffractive imaging using randomly coded masks," *Appl. Phys. Lett.* **107** (2015) 231103.
- [33] M. Stockmar, P. Cloetens, I. Zanette, B. Enders, M. Dierolf, F. Pfeiffer, and P. Thibault, "Near-field ptychography: phase retrieval for inline holography using a structured illumination," *Sci. Rep.* **3** (2013), 1927.
- [34] D. Sylman, V. Micó, J. Garca & Z. Zalevsky, "Random angular coding for superresolved imaging," *Appl. Opt.***49** (2010), 4874-4882.
- [35] P. Thibault, M. Dierolf, O. Bunk, A. Menzel, F. Pfeiffer, "Probe retrieval in ptychographic coherent diffractive imaging," *Ultramicroscopy* **109** (2009), 338-343.
- [36] P. Thibault, M. Dierolf, A. Menzel, O. Bunk, C. David, F. Pfeiffer, "High-resolution scanning X-ray diffraction microscopy", *Science* **321** (2008), 379-382.
- [37] P. Thibault and A. Menzel, "Reconstructing state mixtures from diffraction measurements," *Nature* **494** (2013), 68-71.
- [38] F. Zhang, B. Chen, G. R. Morrison, J. Vila-Comamala, M. Guizar-Sicairos & I. K. Robinson, "Phase retrieval by coherent modulation imaging," *Nat. Comm.* **7** (2016):13367.
- [39] X. Zhang, J. Jiang, B. Xiangli, G.R. Arce, "Spread spectrum phase modulation for coherent X-ray diffraction imaging," *Optics Express* **23** (2015), 25034-25047.
- [40] G. Zheng, R. Horstmeyer and C. Yang, "Wide-field, high-resolution Fourier ptychographic microscopy," *Nature Photonics* **7** (2013), 739-745.

DEPARTMENT OF MATHEMATICS, UNIVERSITY OF CALIFORNIA, DAVIS, CALIFORNIA 95616, USA. EMAIL: FANNJIANG@MATH.UCDAVIS.EDU